Hindawi
Advances in Acoustics and Vibration
Volume 2019, Article ID 7691645, 12 pages
https://doi.org/10.1155/2019/7691645

Research Article

Air Ultrasonic Signal Localization with a Beamforming Microphone Array

Ali Movahed,[1] **Thomas Waschkies**,[2] **and Ute Rabe**[2]

[1] *University of Applied Sciences htw saar, Saarbrücken, Germany*
[2] *Fraunhofer-Institut for Nondestructive Testing IZFP, Campus E3. 1, 66123 Saarbrücken, Germany*

Correspondence should be addressed to Ute Rabe; ute.rabe@izfp.fraunhofer.de

Received 27 August 2018; Revised 16 January 2019; Accepted 24 January 2019; Published 11 February 2019

Academic Editor: Jorge P. Arenas

Nondestructive testing methods are used to inspect and test materials and components for discontinuities or differences in mechanical characteristics. Phased array signal processing techniques have been widely used in different applications, but less research has been conducted on contactless nondestructive testing with passive arrays. This paper presents an application of beamforming techniques analysis using a passive synthetic microphone array to calculate the origin and intensity of sound waves in the ultrasonic frequency range. Acoustic cameras operating in the audible frequency range are well known. In order to conduct measurements in higher frequencies, the arrangement of microphones in an array has to be taken into consideration. This arrangement has a strong influence on the array properties, such as its beam pattern, its dynamics, and its susceptibility to spatial aliasing. Based on simulations, optimized configurations with 16, 32, and 48 microphones and 20 cm diameter were implemented in real experiments to investigate the array resolution and localize ultrasonic sources at 75 kHz signal frequency. The results show that development of an ultrasonic camera to localize ultrasonic sound sources is beneficial.

1. Introduction

Ultrasonic arrays [1] for nondestructive testing (NDT) are well known in industry to detect defects such as cracks or voids in components, flaws in welded joints, or properties such as thickness variations. In most of the NDT applications, linear and planar arrays are implemented in which the same elements are active transmitters and passive receivers of ultrasonic signals. Such phased arrays are deployed to create two-dimensional cross-sectional images, and the sensors have to be in contact with the component surface to perform the measurement, or the component has to be immersed in a coupling medium such as water.

In the field of air acoustics on the other hand acoustic camera systems are increasingly popular for detection, visualization and analysis of sound sources. These systems are based on beamforming, where an array of passive receivers is used to enhance identification of air acoustic emissions by summing the received signals of all microphones with individual delays [2, 3]. The received signals can be multiplied by a weighting factor to suppress the interfering signals at unwanted directions and steer the response of the array. Delay and sum beamforming is a simple broadband method which is advantageous to detect short pulses and transient signals with high computational efficiency [4]. Advanced deconvolution [5, 6] and super resolution [7] methods have been introduced to improve the dynamic range and spatial resolution in the beamforming map. Although recent deconvolution techniques try to extract the strongest source by neglecting the influence of element configuration on the beamforming results and removing some of the artifacts produced by this configuration, in practice the quality of the results will be still impacted by the array [8]. Therefore, it is significant that the array has good performance for the intended beamforming application.

While beamforming with passive acoustic arrays is often used in sonar [9] and seismology [10], there are fewer applications in ultrasonic nondestructive testing. It was shown that beamforming techniques can be used to improve the performance of sensor arrays for acoustic emission monitoring of large concrete structures [11]. Furthermore, the time reversal MUSIC (multiple signal classification) algorithm

which produces high resolution images below the diffraction limit was compared to the total focusing method (TFM) in processing of ultrasonic array data to resolve closely spaced scatterers [12]. The total focusing method requires full matrix capture: each element of the array subsequently sends a pulse into the examined volume, while all elements are simultaneous receivers. The time signals of all channels are individually digitized and stored. After all N elements emitted their pulses, a matrix with N^2 time signals (so-called "full matrix") is available. These data are reconstructed with the synthetic aperture focusing technique (SAFT) which is presently the dominating reconstruction technique for ultrasonic array data in NDT. SAFT is a delay-and-sum based method, which considers the acoustic time-of-flight between the emitter, the receiver, and each pixel/voxel in the reconstruction plane/volume. This reconstruction is called total focusing because it delivers similar or even better results than a classical phased array, which is actively focused on all points of the reconstruction volume. Examples for application of passive air coupled acoustic cameras in NDT are the detection of Lamb waves interacting with impact damage in composite plates [13] and detection of impact echo signals taken of a concrete slab with artificial defects [14]. Furthermore, noise source localization of trains [15], cars [16], airplanes [17], and wind turbines is typical applications of beamforming microphone arrays. However, the conventional air-coupled beamforming systems cannot be applied to the majority of ultrasonic NDT problems due to their frequency limitation. Detectors, digitizers, and element arrangements of commercial acoustic cameras are optimized for signal frequency below 20 kHz. For navigation of robotic systems [18] or as an orientation aid for visually impaired people [19], systems in the ultrasonic frequency range around 40 kHz were developed. It was already pointed out [20] that the higher ultrasonic frequency provides the advantage of better local resolution and less reverberation artifacts. For an application in air-coupled ultrasonic testing, an even higher operating frequency of up to 500 kHz will be needed. The aim of this work is to design and build an air-coupled receiving microphone array for ultrasonic range applications and to examine its performance with real measurements.

2. Array Shape and Design

The arrangement of the microphones is one of the most important factors to enhance the results of beamforming. Knowing the principles of microphone arrays, the optimization of array design parameters makes it possible to investigate configurations that need fewer microphones for a desired application. In this chapter, the theoretical background for array shape selection is explained.

2.1. Array Pattern and Beam Pattern. The response pattern of a passive microphone array with M microphones depends on its individual sensors and on their arrangement in space. The array pattern describes the response of the array to plane waves with wave vector $\vec{k}$ and is defined as follows [2]:

$$W\left(\vec{k}\right) = \sum_{m=1}^{M} w_m^* e^{i\vec{k}\bullet\vec{x}_m} \quad (1)$$

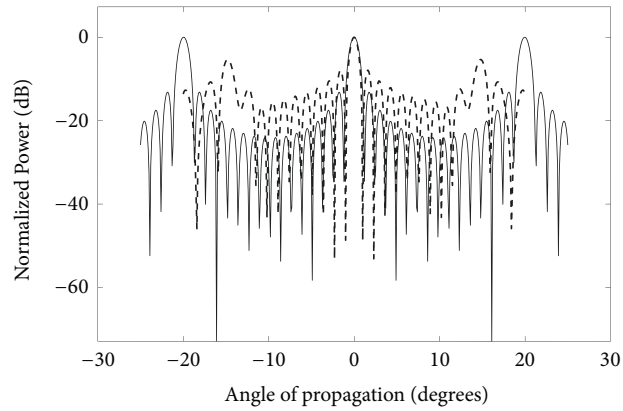

Figure 1: Beam pattern calculated for ring (dashed line) and linear (solid line) arrays at 75 kHz. In order to have good separation between the lobes, small beam width is desired.

where k = $2\pi/\lambda$ is the acoustic wave number, λ is the acoustic wavelength, w_m^* is a complex weight, and $\vec{x}_m$ is the vector position of the m^{th} element with respect to the array origin and m is the number of the m^{th} microphone, m = $\{1, 2, 3, \ldots M\}$. The beam pattern $B(\theta, \varphi)$ is the array response as a function of direction evaluated for a fixed wave number k = $2\pi/\lambda$.

$$B(\theta, \varphi) = \sum_{m=1}^{M} w_m^* e^{ik\vec{u}\bullet\vec{x}_m} \quad (2)$$

Here, the vector $\vec{u}$ is the unit vector from the array origin to the field point. The angles θ and φ indicate the direction of the phase fronts of the incoming radiation, i.e., the direction of $\vec{k} = k\vec{u}$ in a spherical coordinate system. To increase the response of the receiving array in a specific direction $\vec{u} = \vec{u}_0$ of arrival, the complex weights w_m^* can be defined as follows:

$$w_m^* = |w_m| e^{-ik\vec{u}_0\bullet\vec{x}_m} \quad (3)$$

The main array parameters to be taken into account in the array design are explained on a sample beam pattern simulation using a target angle of 0° in Figure 1. This sample was calculated according to (2) by using MATLAB (The MathWorks Inc). The angular behavior in a plane perpendicular to the array plane of a ring with 32 omnidirectional microphones and 20 cm diameter was simulated. For comparison, the beam pattern of a linear array with 20 cm length and 16 omnidirectional microphones is shown. The frequency was set to 75 kHz, which yields a wave length λ = 4.6 mm in air (sound velocity 343 m/s). The weights and array element field pattern were set to one. The lobe centered on the target angle of 0° is called the main beam. The difference between the two minima on either side of the main beam defines the null-to-null beam width. The width of the main lobe at -3dB is called the half power beam width and the difference between the main lobe and maximum power of the first side lobe is called maximum side lobe level (MSL). The beams of equal magnitude appearing at the angles of 20° and -20° in the beam

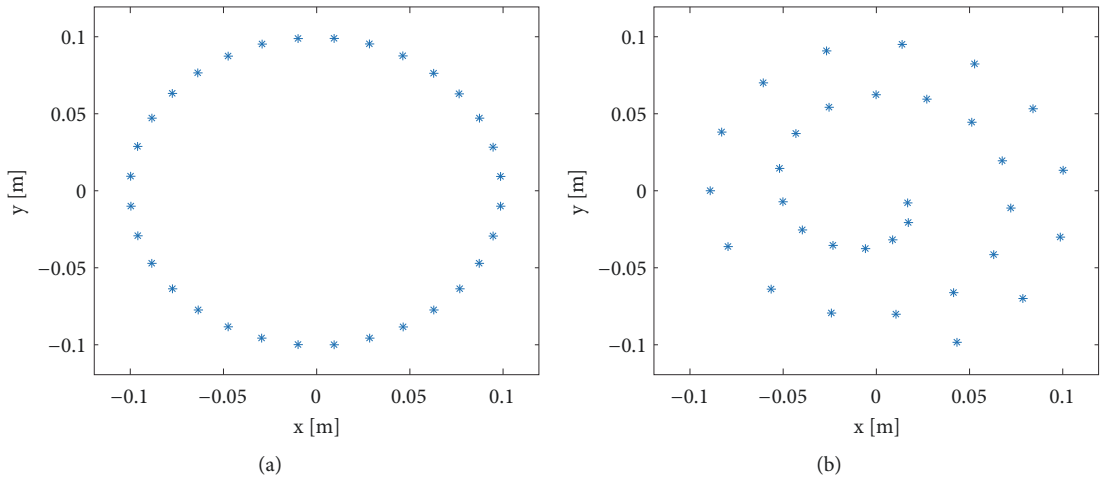

Figure 2: (a) Ring array with 32 elements and (b) spiral V = 8.2 array with 32 elements and 20 cm diameter.

pattern of the line array and the beams at the angles of 15° and -15° in the beam pattern of the ring array are grating lobes. Grating lobes appear, e.g., in the linear array when the distance between the microphones is larger than $\lambda/2$ [21]. Figure 1 shows that the linear array has a lower MSL than the ring array but strong grating lobes.

The width of the main lobe defines the array resolution which is a significant parameter that affects the sound source localization results and is influenced by the array geometry. The Rayleigh criterion is a well-known definition of resolution at the diffraction limit which was first defined in optics [22]. According to this criterion, two waves are considered just resolved when the maximum of the diffraction pattern of the first source is detected at the first minimum of the second source. The respective equation for linear arrays (l) and circular apertures (c) (and microphone arrays) is given by the following [3]:

$$\theta_{R_l} = \frac{\lambda}{\mathrm{L}} \tag{4}$$

$$\theta_{R_c} = 1.22\frac{\lambda}{\mathrm{D}} \tag{5}$$

where θ_R is the resolved angle at the Rayleigh limit, λ is the wavelength of the source, L is the length of the linear array, and D (5) is the diameter of the circular array. As the Rayleigh angle is small, the approximation $\theta_R \approx \varepsilon_R/d$ can be used, where ε_R is the distance between the two sources and d is the distance between the source and the array. Equation (5) shows that the resolution improves with larger array diameters but becomes worse when the measurement distance or the wavelength is increased.

In order to optimize the application of the microphone arrays, it is important to have good source separation and as low as possible levels of the side lobes, which means that large diameters would be preferred. On the other hand, it is important to have small microphone spacing to achieve a wide angle between the side lobes or to avoid side lobes when analyzing high frequencies. To overcome this, a variety of microphone configurations (linear, cross-shape, periodic grid, circle, and spiral) have been investigated in the literature [23] to report that circular and spiral arrangements have more benefits than the other geometries. Taking this into account, and a moderate amount of receiving channels, we considered a ring and a sunflower spiral [24] with M = 32 microphones for our measurements.

2.2. Spiral Array Selection. Higher frequency means lower wavelength and it therefore increases local resolution. On the other hand, the attenuation of airborne sound increases with increasing frequency. For a first demonstration we therefore chose a center frequency of 75 kHz which is clearly in the ultrasonic range but still low enough such that special wide-band microphones are available. In order to attain a resolution ε_R in the mm range at source, array distance d of several 10 cm, we chose a diameter D of 20 cm. The sunflower spiral formula describes different spiral configurations with a fixed number of elements depending on a parameter V. This formula in polar coordinates is given by the following [25, 26]:

$$F(m) = \left(r_m(m), \theta_m(m)\right) = \left(\sqrt{m}, 2\pi m\frac{\sqrt{V}-1}{2}\right) \tag{6}$$

where $\mathrm{r_m}$ and θ_m are the polar coordinates of the $\mathrm{m^{th}}$ element with respect to the array origin, and V is the corresponding parameter to each unique configuration. Different values of V lead to different possible arrangements such as multi-armed spirals and linear configurations. The configurations are all different, if V varies in steps of 0.1 in a range between 1 and 9. We analyzed beam patterns of the arrangements with V from 1 to 9 (step size 0.1) at 75 kHz and calculated the MSL of each V. Among all the configurations, V = 3.2 and V = 8.2 showed the best MSL, -10.39 and -10.15 dB, respectively [27]. The single-armed spiral with parameter V = 8.2 was selected here for further evaluation, because the spacing between all microphone positions is different. An arrangement with high symmetry and equal microphone spacing, a ring configuration, serves for comparison. The two arrays, chosen for further investigations in the ultrasonic frequency range, are shown in Figure 2.

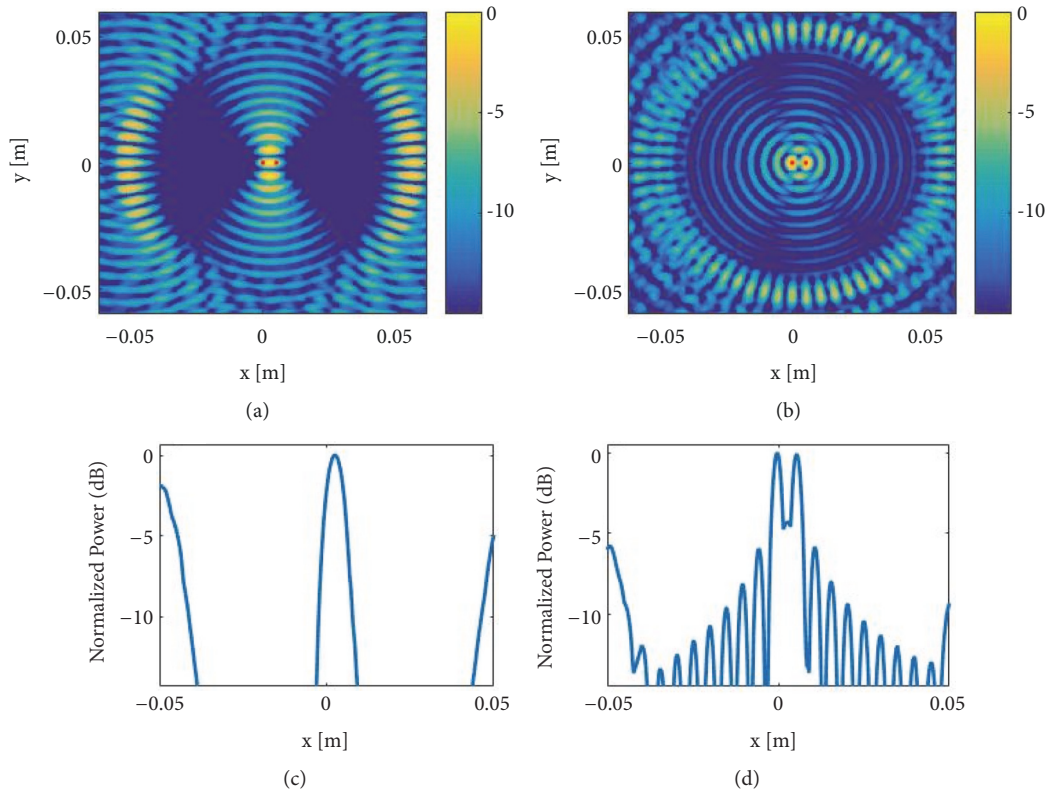

Figure 3: Simulated reconstruction result with sum and delay beamforming for a ring array with 32 elements (Figure 2(a)) at a distance of 18 cm from two point sources which are separated by 5 mm. (a) The sources are two spherical waves at 75 kHz. (c) The sources are spherical waves at 74 and 76 kHz, respectively. (b), (d) Cross section of (a) and (c) at y = 0. Red dots show the position of the sources.

3. Simulation and Beamforming

According to the Rayleigh criterion in (5), two sources at 75 kHz frequency with a separation of $\varepsilon_R = 5$ mm (center-to-center) can be resolved with a ring array of 20 cm diameter, which is 18 cm far from the source plane. Generally, the Rayleigh resolution limit is only applicable when the signals are not in phase [28]. Furthermore, simple formulas are only available for selected microphone configurations like rings and lines. Therefore, we simulated the signals of two point sources with a separation ε_R = of 5 mm with equal frequency (75 kHz) and with slightly different frequencies (74 kHz and 76 kHz). We defined spherical waves as our sources which have the following form:

$$A\left(\vec{d},t\right) = A_0 \frac{e^{i(\vec{k}\,\vec{d}-\omega t)}}{d} \tag{7}$$

where A_0 is an amplitude and is the vector distance from the source location to the microphone, $d = |\vec{d}|$, and $\omega = 2\pi/\lambda$ is the angular frequency of the spherical wave. The amplitudes as a function of time $f_m(t)$ for the M microphones with positions according to Figures 2(a) and 2(b) were produced by summation over the signals of the sources at different chosen positions. The microphones and the sound sources are arranged in plane configurations parallel to each other. The distance between the source plane and the microphone plane is 18 cm. The simulated data were reconstructed with the delay and sum method. The basis of sum and delay beamforming is to calculate the relative delays from the points on the surface of a sound emitting object to each microphone in the array. The reconstruction function in time domain for the points in the image plane is given by the following [4]:

$$f\left(\vec{X},t\right) = \frac{1}{M}\sum_{m=1}^{M} f_m\left(t-\Delta_m\right) \tag{8}$$

where $\vec{X}$ is the vector position of the point in the reconstruction plane, f_m is the recorded time signal of the m$^{\text{th}}$ microphone, and Δ_m is the relative delay. The relative delays are calculated from the absolute delays (τ_m) according to $\Delta_m = \tau_m - \min(\tau_m)$. The absolute delays have the form $\tau_m = d_m/\mathrm{c}$, where c is the sound velocity, $\vec{d_m}$ is the vector distance between each microphone in the array and the points in the image plane, and $|\vec{d_m}| = d_m$. The aforementioned conventional beamforming algorithm is the oldest and most popular signal processing algorithm. As it is well suited for pulsed signals, it was employed here to localize ultrasonic and acoustic sources in simulations and real experiments.

Figures 3(a) and 4(a) show the absolute field of the reconstruction results of the two point sources with equal frequency and with slightly different frequencies (Figures 3(c) and 4(c)) using the ring and the spiral array with 32

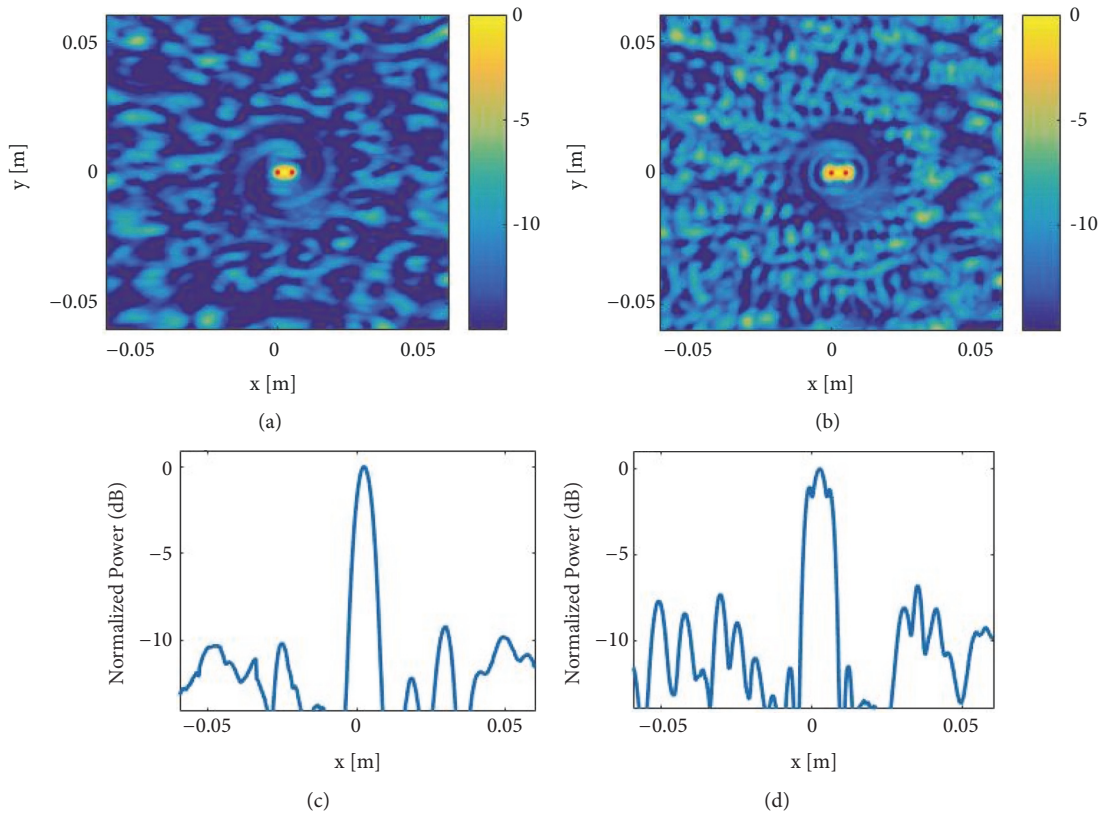

FIGURE 4: Simulated reconstruction result by sum and delay beamforming for a V = 8.2 spiral array with 32 elements (Figure 2(b)). The spiral is located at a distance of 18 cm from two point sources, which are separated by 5 mm. (a) Point sources are two spherical waves at 75 kHz. (c) Point sources are spherical waves at 74 and 76 kHz, respectively. (b), (d) Cross section of (a) and (c) at y = 0. Red dots show the position of the sources.

microphones as shown in Figures 2(a) and 2(b), respectively. The results are displayed with a -15 dB dynamic range for all cases, and the size of the reconstruction plane is 60 mm × 60 mm (height × width). As it can be seen from Figure 1, the grating lobes of the ring array appear at the angle of 15°, which is equal to 47.12 mm when the source is 18 cm far from the array. Therefore, our chosen reconstruction plane covers the whole area of interest. The distance between each pixel in x- and y-directions is 0.3 mm. This is even more than 10 times smaller than the wavelength of the source (4.57 mm). The distance between the microphones and the reconstruction plane is 18 cm. The graphs below the images show a cross section of the data at y = 0. As can be seen in Figures 3(c) and 4(c), the sources which are out of phase are resolved by the ring array and by the spiral array. As expected, the spiral array exhibits a slightly lower local resolution. On the other hand, the ring array produces strong artefacts and side-lobes especially in case of in-phase sources (Figure 3(a)), while the spiral array still locates the in-phase sources though being merged to one point (Figure 4(a)). In addition, the spiral has a much lower side lobe level than the ring. The separate localization of coherent sources is of relevance for NDT testing applications, because in the typical NDT testing situation the objects are actively excited to vibration with a fixed frequency and phase. As both array types have their advantages and disadvantages, ring and spiral were both used in the experiments.

4. Experimental Results

In order to evaluate the performance of the array design, experimental tests were conducted in the ultrasonic frequency range at 75 kHz and for comparison also in the acoustic frequency range at 10 kHz and 20 kHz. In both cases the sound source was placed behind a screen with two apertures of 1 cm diameter and a center-to-center separation of 15 mm. A commercial acoustic camera with 48 microphones was available for the experiment in the acoustic frequency range. For the experiment in the ultrasonic frequency range, a single microphone in combination with a mechanical positioning device was used to collect the data at the 32 microphone positions as depicted in Figure 2.

4.1. Measurement with the Acoustic Camera. In order to examine the resolution in the acoustic frequency range, we conducted measurements with a commercial acoustic camera (Gfai tech GmbH, Berlin, Germany). A Bluetooth speaker was placed in a wooden box with two holes of 1 cm diameter and 1.5 cm center-to-center separation. The speaker was excited with 10 kHz and 20 kHz continuous wave sinus signals

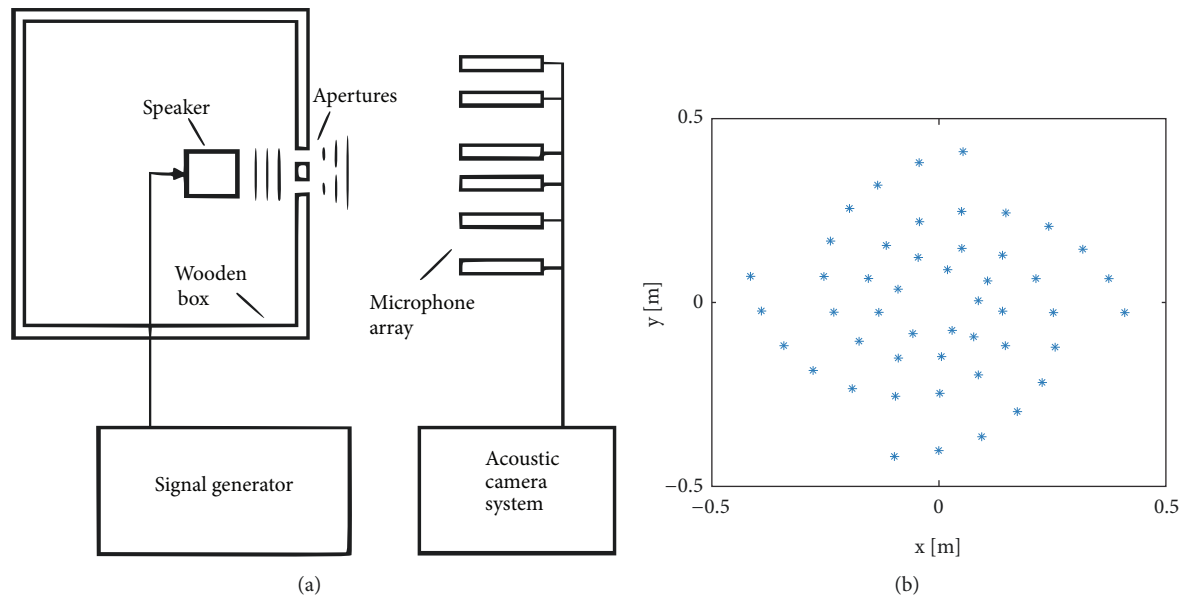

FIGURE 5: (a) Schematic set-up of the measurement; (b) the spiral configuration of the commercial microphone array.

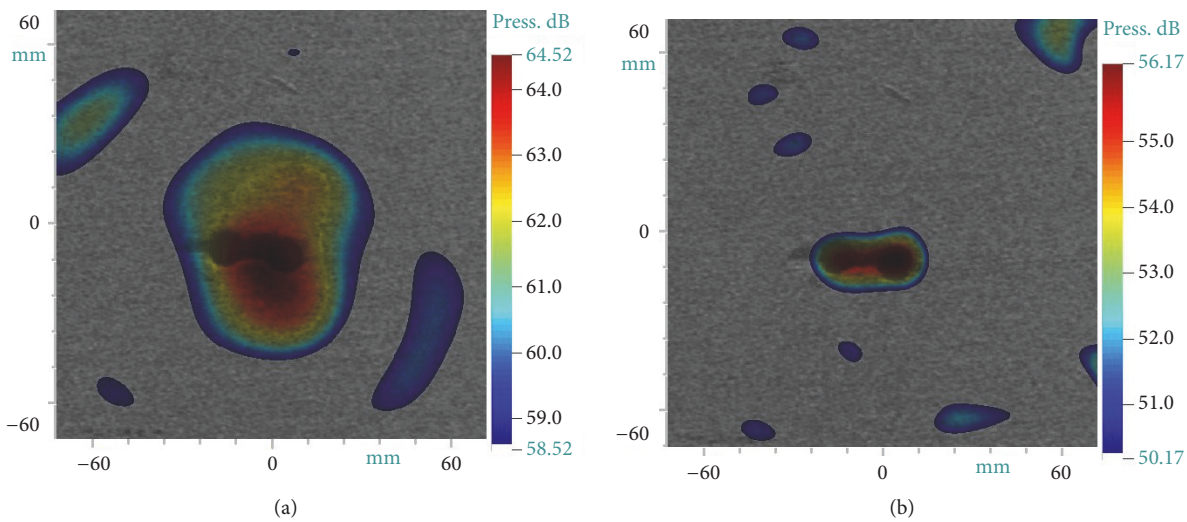

FIGURE 6: Source localization with the acoustic camera (spiral configuration). (a) at 10 kHz; (b) at 20 kHz.

from a signal generator. A commercial 48-channel planar spiral configuration (83 cm diameter) and a ring configuration (75 cm diameter) with data acquisition and evaluation unit were used to detect and localize the signals coming from two holes (Figure 5). The camera was placed at a distance of 40 cm from the holes. The signals of the 48 microphones in the frequency band from 20 Hz to 20 kHz (± 3dB) were stored and processed with the commercial software in frequency domain beamforming. The measurement was done with a 192 kHz sampling rate, and the acquired time interval was 1 second. Figures 5 and 6 depict the localized acoustic signal with the available ring and spiral configurations in a color code image superimposed to an optical photo taken with a digital camera in the center of the array. According to the Rayleigh criterion discussed in Section 2, the minimum distance between two sources, which will be resolved by a circular aperture of 83 cm diameter, is 1.00 cm and 2.01 cm, respectively, at 20 kHz and 10 kHz frequency. Although the holes are 1.5 cm far from each other, the spiral does not resolve them as two sources, as can be clearly seen in Figure 6. In comparison, the ring configuration is able to localize two separate sources at 20 kHz which is in agreement with the simulations that a ring has a slightly better resolution than a spiral. As the Rayleigh limit cannot be calculated with simple analytical formulas for spirals or other nonperiodic configurations, it is more convenient to use amplitude thresholds to evaluate resolution. Well-known limits are the 3-dB (half power) or the 6-dB levels [2, 12]. Due to this, we displayed the result of the acoustic camera with a 6 dB dynamic range which outlines the sources not resolved. The results presented in Figures 5–7

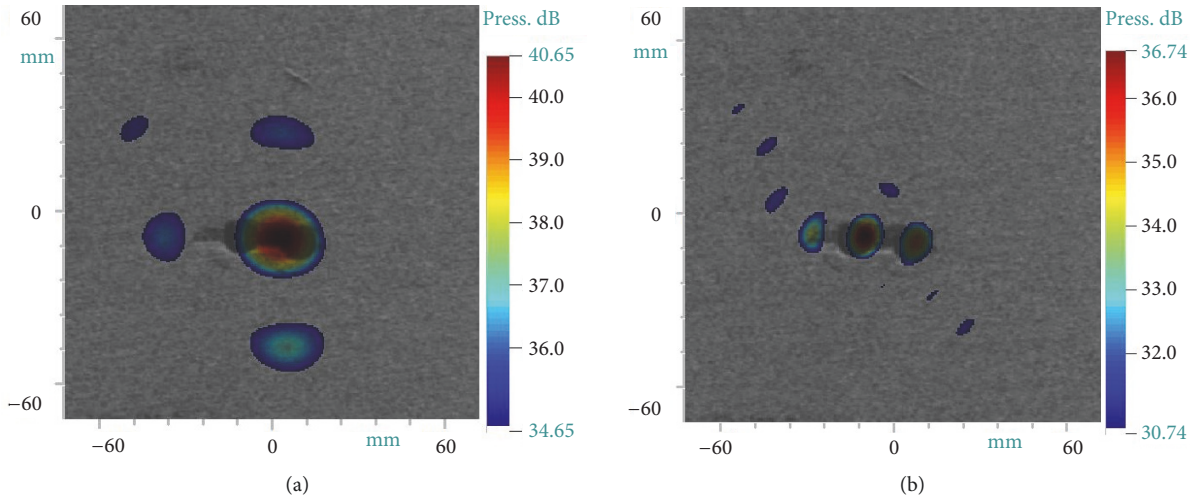

Figure 7: Source localization with the acoustic camera (ring configuration). (a) at 10 kHz; (b) at 20 kHz.

were obtained by frequency domain beamforming. Furthermore, we analyzed the data in time domain beamforming, which delivered a lower local resolution and a high noise level from background signals.

Theoretically, the angular resolution would improve when the acoustic array would be positioned closer to the source, but because of the diameter of the arrays of 83 cm and 75 cm, a distance to the object below 40 cm would not improve the reconstruction result but leads to source localization instability. Experimentally, it is not recommended to perform the measurement closer than the diameter, but the localization may even work to a certain distance.

The appearance of the side lobes around the main lobe especially in Figure 7(a) is due to the big interelement spacing in the array. The resolution can be improved by increasing the frequency of the sound source or by increasing the size of the array. Increasing the size of the array will lead to a bigger element distance which produces more artefacts. Increasing the number of microphones while increasing the diameter of the array will lead to more costs for the acquisition system. Therefore, it is more practical to have a dense microphone array even with fewer microphones to be able to localize higher frequencies and decrease the costs.

4.2. Measurement with the Passive Synthetic Ultrasonic Microphone Array. For the experiment in the ultrasonic frequency range, an ultrasonic transducer with 6 cm aperture and a center frequency of 75 kHz (15% bandwidth) was used to send the signals. A schematic set up is shown in Figure 8. The transducer was placed 6.5 cm behind a 3 mm thick corrugated cardboard screen with two holes of the same size and distance as those in the wooden box for the acoustic experiment (1 cm diameter, 1.5 cm center-to center-separation). The transducer was exited with a 75 kHz sinus burst signal with 3 cycles and 220 V sending voltage. Sinus burst signals are the typical type of excitation for air ultrasonic transducers. They are a compromise between a single frequency and a pulsed

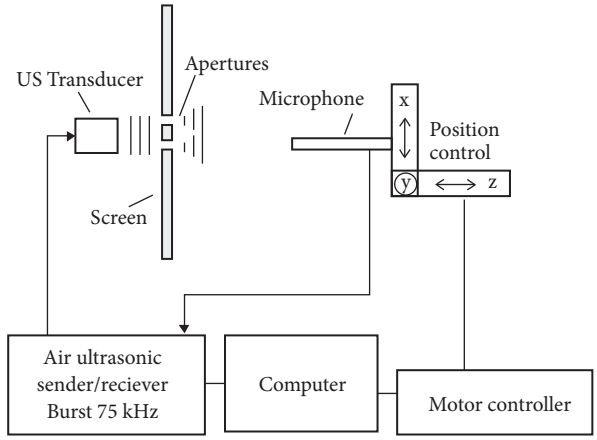

Figure 8: Schematic set-up of the measurement in the ultrasonic frequency range.

excitation. A continuous wave measurement would damage the transducers due to the high average power.

To detect the direction of the sources defined by the holes an ultrasonic receiving array is needed. For the experiments which will be presented here, we employed a broadband microphone with a constant sensitivity up to 100 kHz frequency and a diameter of 3 mm (Type 40 DP, 1/8" Pressure Microphone, G.R.A.S. Sound & Vibration, Denmark). The microphone was mounted to a motorized 3-axis mechanical positioning device which was located in front of the screen. While the distance to the screen (z-coordinate) was kept constant, the microphone was moved in x and y directions with a manipulator to 32 specific positions to build the passive synthetic spiral and ring arrays.

One of the obstacles when designing high frequency microphone arrays is the small interelement spacing. For the choice of the array configurations (see Section 2.2) we considered the microphone dimensions, such that the minimum interelement spacing was always larger than the

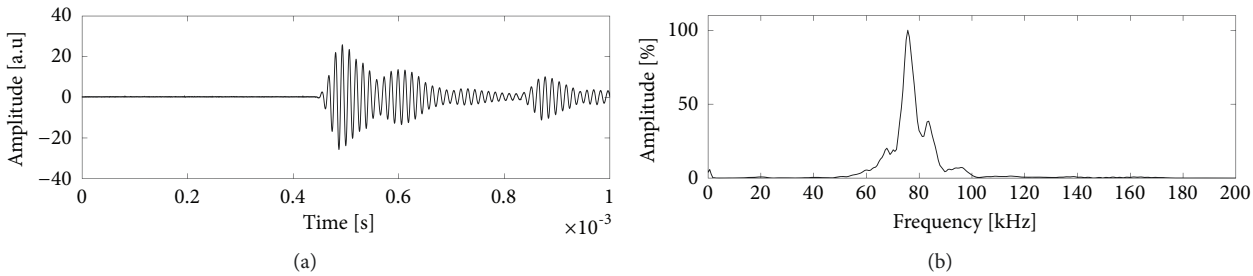

FIGURE 9: (a) Recorded time signal of the first microphone at the spiral positions (V = 8.2) at 0.9 D distance from the source and (b) averaged spectra of the time signals calculated by fast Fourier transformation.

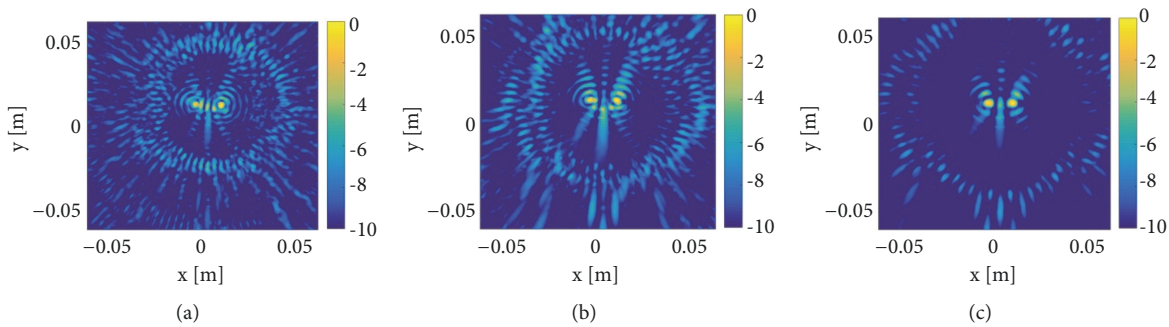

FIGURE 10: Beamforming result at 75 kHz frequency calculated from the experimental data acquired with the synthetic ring array with 32 elements. Z-distance of the microphone to the screen: (a) 0.5 D; (b) 0.65 D; (c) 0.9 D.

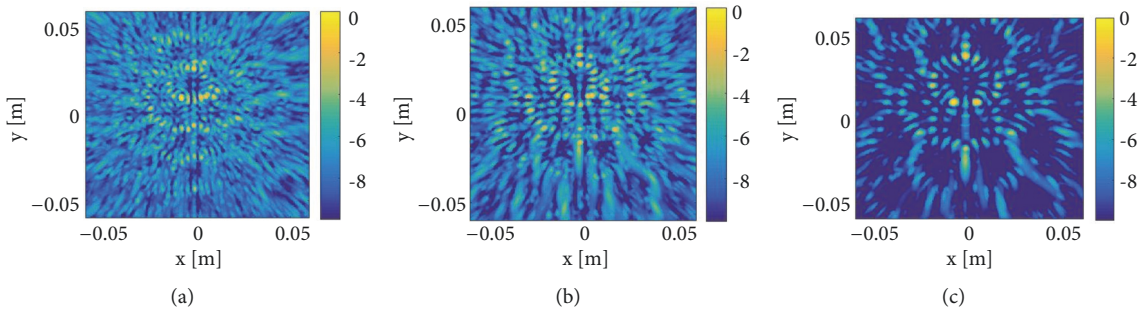

FIGURE 11: Beamforming result at 75 kHz frequency calculated from the experimental data acquired with the synthetic spiral array (V = 8.2) with 32 elements. Z-distance of the microphone to the screen: (a) 0.5 D; (b) 0.65 D; (c) 0.9 D.

diameter of the microphone. The diameter of the arrays with 32 microphones was 20 cm, and the smallest distance between two microphone positions was 0.98 cm (2.14λ) in the spiral configuration and 1.96 cm (4.28λ) in the ring configuration.

The ultrasonic time signal of each position was captured, digitized, and stored in a computer. A sampling frequency of 20 MS/s was chosen; the length of the time interval was 1 ms. For each microphone configuration, the measurement was performed at three different screen–microphone distances, 0.5 D, 0.65 D, and 0.9 D, respectively, to investigate ultrasound localization at distances less than the diameter of the array (D = 20 cm). The shorter distances were chosen for comparison because ultrasonic sources have short wavelength which increases the attenuation as a function of distance. As an example for a typical shape of the received signals, the time signal captured with the first microphone of the spiral V = 8.2 from the origin at 0.9 D measurement distance and the averaged frequency spectra of the signals of all microphones calculated by fast Fourier transformation are depicted in Figure 9. The first microphone is the microphone with the smallest x and y coordinates in the center of the spiral in Figure 2(b).

With a program written in MATLAB, the experimental data were delayed and summed to perform the time domain localization as explained in Section 3 (8). The results calculated with the 32 signals obtained with the ring and spiral configurations are demonstrated in Figures 10 and 11 for the three different measurement distances. It can be seen that the arrays have the expected performance in agreement with the simulations in Section 3. The ring with 32 elements delivers

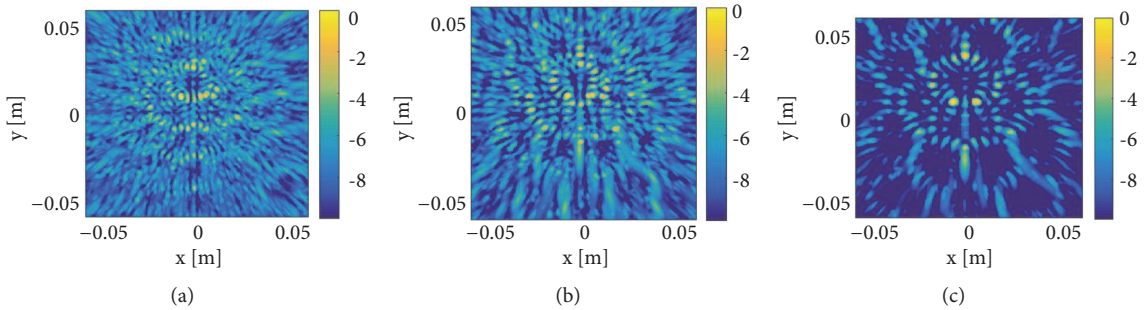

Figure 12: Beamforming result at 75 kHz frequency calculated from the experimental data acquired with the synthetic ring array with 16 elements. Z-distance of the microphone to the screen: (a) 0.5 D; (b) 0.65 D; (c) 0.9 D.

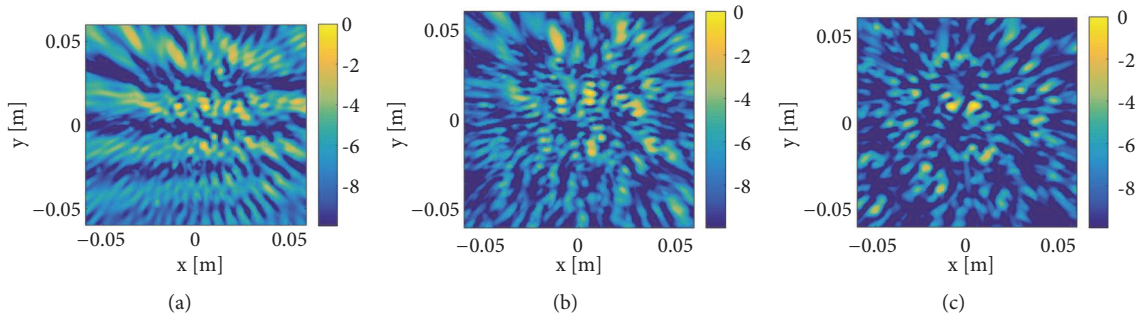

Figure 13: Beamforming result at 75 kHz frequency calculated from the experimental data acquired with the synthetic spiral array (V = 8.2) with 16 elements. Z-distance of the microphone to the screen: (a) 0.5 D; (b) 0.65 D; (c) 0.9 D.

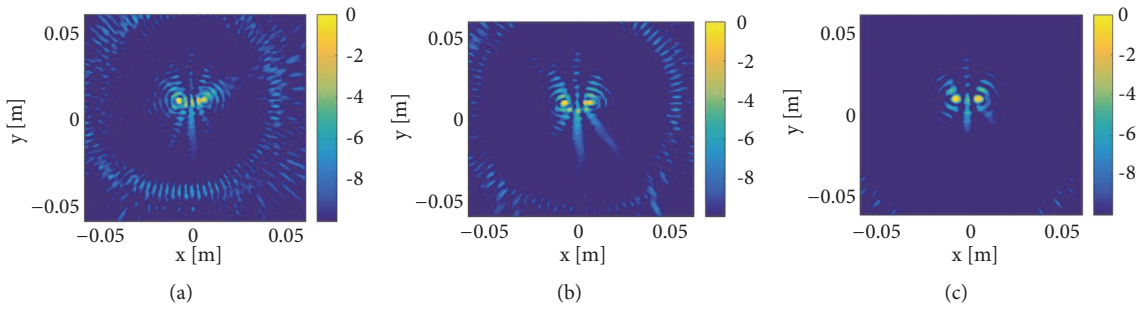

Figure 14: Beamforming result at 75 kHz frequency calculated from the experimental data acquired with the synthetic ring array with 48 elements. Z-distance of the microphone to the screen: (a) 0.5 D; (b) 0.65 D; (c) 0.9 D.

better resolution, but more side lobes. There is an extreme appearance of artefacts in the reconstruction plane when the array is placed very close (0.5 D) to the source which makes it difficult to find the exact position of the holes. To examine the influence of the distance of the array to the source, the distance of the microphone from the screen was increased to 0.65 D and 0.9 D. The best results were achieved when the measurement distance was 0.9 D, a bit less than the diameter of the arrays.

To get a better overview, we repeated the measurements with 16 and 48 microphone positions and kept the diameter of the arrays constant to 20 cm. Figures 12–15 depicts the reconstruction results. The reconstruction images with 16 microphones especially at smaller measurement distances are not reliable, which make it difficult to find the exact position of the sources. On the other hand, arrays with 48 microphones demonstrate precise localization. The calculation with 48 microphones demands more computation time and memory capacity, which is unfavorable for most of the applications. To analyze these results quantitatively, we measured MSL and API (array performance indicator) from Figures 10–15. The results of this analysis are shown in the Table 1. API is a dimensionless measure of the resolution of the microphone arrays, which is defined as the area of a source calculated at -6 dB from its peak, divided by the square of the wavelength [12]. The beam width in the field of acoustic source localization is defined as the width of the main beam at -3 dB. Therefore, we calculated the area of each source at -3 dB from its maximum value and added these values to find API for each case in Table 1. It can be seen from the table that

Table 1: Results of post processing experimental data.

Ring	16 Microphones		32 Microphones		48 Microphones	
d	MSL (dB)	API	MSL (dB)	API	MSL (dB)	API
0.5 D	-	-	-0.20	0.65	-0.25	0.66
0.65 D	-	-	-2.00	0.74	-1.50	0.75
0.9 D	-0.89	1.08	-4.10	1.10	-4.10	1.12
Spiral 8.2	16 Microphones		32 Microphones		48 Microphones	
d	MSL (dB)	API	MSL (dB)	API	MSL (dB)	API
0.5 D	-	-	-1.45	1.54	-4.10	1.67
0.65 D	-	-	-4.40	1.65	-6.00	1.68
0.9 D	-2.24	2.00	-5.65	1.89	-6.20	1.94

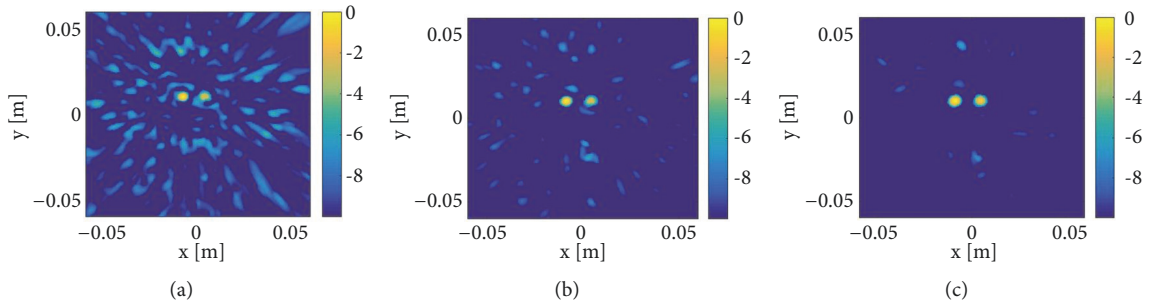

Figure 15: Beamforming result at 75 kHz frequency calculated from the experimental data acquired with the synthetic spiral array (V = 8.2) with 48 elements. Z-distance of the microphone to the screen: (a) 0.5 D; (b) 0.65 D; (c) 0.9 D.

API increases with an increase in the number of microphones except the case with 16-microphone spiral arrangement at 0.9 D, which delivers a high value. After a closer look at this reconstruction, it was seen that the area of right source at -3 dB is extended and seems bigger. This could happen because of a calculation with a smaller number of microphones. Moreover, the reconstruction with 16 microphones at short measurement distances is not trustworthy and the images fail to deliver reasonable values for MSL and API. The MSL of the ring array does not improve even with large number of microphones; however, spiral array gains better MSL with 48 microphones, mostly at long measurement distances. In general, the MSL difference between 32 and 48 microphones is not abundant and a smaller number of microphones lead to better resolution.

In order to make sure that the two maxima obtained by beamforming in Figures 10–15 are not caused by aliasing or by side lobes but can be attributed to the two real sources, we repeated the measurements with single sources by covering one of the holes. Figure 16 shows the result when the left and the right hole were covered, respectively. In this case, just one of the sources is visible in each measurement. As the measurement set-up was moved a small amount to one side, both sources are shifted to the left compared to the results in Figures 10–15. We measured the x-position corresponding to the center of each peak in Figure 16. The center-to-center distance between the peaks is 13 mm, which is close but not exactly equal to the expected 15 mm. The reason for the deviation could be in the experimental set-up as well as in the properties and position of the spiral and will have to be examined in future. The experiments presented in Figures 10–15 clearly show that the source localization at 75 kHz frequency was successful and sources with the

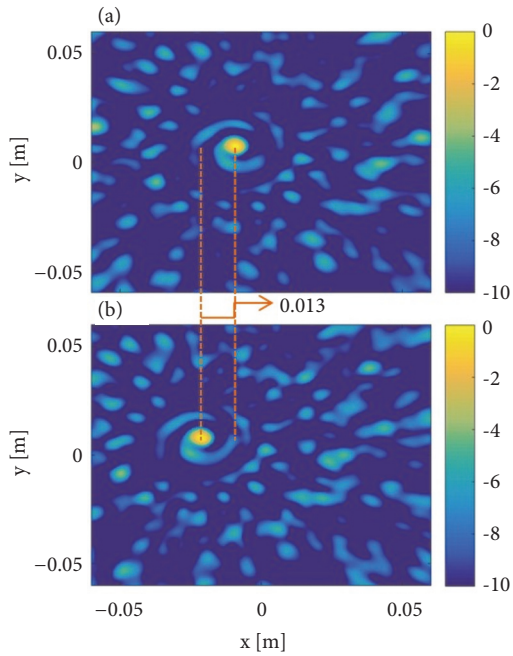

Figure 16: Beamforming result at 75 kHz frequency, calculated with experimental data from the spiral configuration at 18 cm distance from the screen. (a) Left hole covered; (b) right hole covered.

separation distance less than 15 mm can be resolved. In addition to the delay and sum beamforming in the time domain, we also tested frequency domain beamforming with the experimental data. The frequency domain beamforming showed stronger side lobe levels. For this reason, these results are not shown.

5. Conclusion and Future Work

This research work presents first steps towards an ultrasonic microphone array for NDT applications. Ring and spiral configurations with 32 elements and 20 cm diameter were designed and simulated to examine the array resolution and localize ultrasonic sources at 75 kHz. The simulations demonstrated that the ring array outperforms the spiral array with respect to the resolution but delivers more artefacts especially in case of two coherent sources. A set of experiments in the ultrasonic frequency range at 75 kHz was performed to corroborate the simulations. As ultrasonic multichannel data acquisition systems would be expensive, we performed the ultrasonic experiments in this study with a single microphone and a single data acquisition system. This microphone was moved to the required positions with the help of a motor driven mechanical positioning system. A screen with two holes with 15 mm center-to-center separation distance placed in front of an ultrasonic transducer was used as the test source. Delay and sum beamforming in time domain served as a simple method for the simulations and for the processing of the ultrasonic experimental data. The measurement at 0.9 D distance between array and screen showed very good results without extreme appearance of side lobes. The number of microphones is very important as it defines the necessary number of channels of the electronics and therefore the overall costs of the system. A comparison to the performance of ring or spiral systems with 16 and 48 microphones showed that 32 microphones are a good compromise at the chosen geometrical conditions.

In order to demonstrate the influence of the operating frequency, a source with the same geometry (a screen with two holes with a center-to-center separation distance of 15 mm) but with lower frequency (10 kHz and 20 kHz) was examined with a commercial acoustic camera equipped with 48 microphones. The best result was obtained with frequency domain beamforming in this case. Nevertheless, it was clearly demonstrated that higher frequency provides higher local resolution as even sophisticated post-processing cannot compensate for all artefacts and broadening effects.

The results of this study have shown that source localization by beamforming is possible in the ultrasonic frequency range above 40 kHz, and that it is possible to improve the local resolution by using ultrasonic frequency. In future studies, the influence of parameters such as measurement distance, array configuration, pulse length, and frequency ranges will have to be investigated and optimized in more detail. Localization of ultrasonic sources with arrays could be very promising in the context of NDT as for example in leakage detection in automotive or aerospace industry. Industrial processes such as welding processes for example do not only emit acoustic signals but also signals in the ultrasonic frequency range. Process monitoring at increased frequency could benefit from a higher signal to noise ratio due to a lower level of reverberation and environmental noise signals as well as a higher local resolution. This could be exploited by application of passive contactless ultrasonic arrays.

Data Availability

The measured MATLAB data used to support the findings of this study are available from the corresponding author upon request.

Disclosure

Some parts of the work were presented as an oral presentation at DAGA Conference 2018 in Munich and Fraunhofer Vision Technologietag 2018 in Jena.

Conflicts of Interest

The authors declare that they have no conflicts of interest.

Acknowledgments

A part of this work has been funded by the German Ministry of Economics and Technology in the frame of the program ZIM (Zentrales Innovationsprogramm Mittelstand), contact ZF4234102LT6, cooperative project BeamUS500, and IZFP project part BeamUS500-Sensor. The authors gratefully acknowledge Nico Brosta and Katharina Bonaventura for helping with ultrasonic data acquisition and MATLAB programming.

References

[1] B. W. Drinkwater and P. D. Wilcox, "Ultrasonic arrays for non-destructive evaluation: a review," *NDT & E International*, vol. 39, no. 7, pp. 525–541, 2006.

[2] H. L. Van Trees, "Optimum array processing," in *Part IV of Detection, Estimation and Modulation Theory*, Wiley, New Dehli, India, 2002.

[3] D. H. Johnson and D. E. Dudgeon, *Array Signal Processing, Concepts and Techniques*, Prentice Hall, Upper Saddle River, 1993.

[4] O. Jaeckel, "Strengths and weaknesses of calculating beamforming in the time domain," in *Proceedings of the Berlin Beamforming Conference (BeBeC)*, 2006.

[5] P. Sijtsma, "CLEAN based on spatial source coherence," in *Proceedings of the 13th AIAA/CEAS Aeroacoustics Conference (28th AIAA Aeroacoustics Conference)*, Italy, May 2007.

[6] T. Brooks and W. Humphreys, "A deconvolution approach for the mapping of acoustic sources (DAMAS) determined from phased microphone arrays," in *Proceedings of the 10th AIAA/CEAS Aeroacoustics Conference*, Manchester, Great Britain, 2004.

[7] R. Schmidt, "Multiple emitter location and signal parameter estimation," *IEEE Transactions on Antennas and Propagation*, vol. 34, no. 3, pp. 276–280, 1986.

[8] Z. Prime and C. Doolan, "A comparison of popular beamforming arrays," in *Proceedings of the Annual Conference of the Australian Acoustical Society, Victor Harbor, Australia*, Red Hook, NY, USA, 2013.

[9] S. D. Somasundaram, N. R. Butt, A. Jakobsson, and L. Hart, "Low-complexity uncertainty-set-based robust adaptive beamforming for passive sonar," *IEEE Journal of Oceanic Engineering*, pp. 1–17, 2015.

[10] E. Ruigrok, S. Gibbons, and K. Wapenaar, "Cross-correlation beamforming," *Journal of Seismology*, vol. 21, no. 3, pp. 495–508, 2017.

[11] G. C. McLaskey, S. D. Glaser, and C. U. Grosse, "Beamforming array techniques for acoustic emission monitoring of large concrete structures," *Journal of Sound and Vibration*, vol. 329, no. 12, pp. 2384–2394, 2010.

[12] C. Fan, M. Caleap, M. Pan, and B. W. Drinkwater, "A comparison between ultrasonic array beamforming and super resolution imaging algorithms for non-destructive evaluation," *Ultrasonics*, vol. 54, no. 7, pp. 1842–1850, 2014.

[13] H. Pfeiffer, M. Böck, I. Pitropakis et al., "Identification of impact damage in sandwich composites by acoustic camera detection of leaky lamb wave mode conversions," *e-Journal of Nondestructive Testing (NDT)*, pp. 1435–4934, 2013.

[14] R. Groschup and C. U. Grosse, "Enhancing air-coupled impact-echo with microphone arrays," in *Proceedings of the International Symposium Non-Destructive Testing in Civil Engineering*, Berlin , Germany, 2015.

[15] B. Barsikow, W. F. King III, and E. Pfizenmaier, "Wheel/rail noise generated by a high-speed train investigated with a line array of microphones," *Journal of Sound and Vibration*, vol. 118, no. 1, pp. 99–122, 1987.

[16] U. Michel and B. Barsikow, "Localisation of sound sources on moving vehicles with microphone arrays," in *Proceedings of EuroNoise*, Naples , Italy, 2003.

[17] U. Michel, B. Barsikow, B. Haverich et al., "Investigation of airframe and jet noise in high-speed flight with a microphone array," in *Proceedings of the 3rd AIAA/CEAS Aeroacoustics Conference*, Atlanta, GA, USA, 1997.

[18] M. Yang, S. Hill, and J. Gray, "Localization of plane reflectors using a wide-beamwidth ultrasound transducer arrangement," *IEEE Transactions on Instrumentation and Measurement*, vol. 46, no. 3, pp. 711–716.

[19] S. Harput and A. Bozkurt, "Ultrasonic phased array device for acoustic imaging in air," *IEEE Sensors Journal*, vol. 8, no. 11, pp. 1755–1762, 2008.

[20] V. Kunin, M. Turqueti, J. Saniie, and E. Oruklu, "Direction of arrival estimation and localization using acoustic sensor arrays," *Journal of Sensor Technology*, vol. 01, no. 03, pp. 71–80, 2011.

[21] F. J. Pompei and S. Wooh, "Phased array element shapes for suppressing grating lobes," *The Journal of the Acoustical Society of America*, vol. 111, no. 5, p. 2040, 2002.

[22] L. Rayleigh, "XXXI. Investigations in optics, with special reference to the spectroscope," *Philosophical Magazine*, vol. 8, no. 49, pp. 261–274, 1879.

[23] A. Nordborg, J. Wedemann, and L. Willenbrink, "Optimum array microphone configuration," in *Proceedings of the 29th International Congress and Exhibition on Noise Control Engineering*, Nice, France, 2000.

[24] H. Vogel, "A better way to construct the sunflower head," *Mathematical Biosciences*, vol. 44, no. 3-4, pp. 179–189, 1979.

[25] H. Segerman, "The sunflower spiral and the fibonacci metric," in *Proceedings of the Bridges: Mathematics, Music, Art, Architecture, Culture*, pp. 483–486, University of Texas at Austin, 2010.

[26] E. Sarradj, "A generic approach to synthesize optimal array microphone arrangements," in *Proceedings of the Berlin Beamforming Conference (BeBeC)*, 2016.

[27] A. Movahed, T. Waschkies, and U. Rabe, "Comparison of different microphone arrays for signal processing of air-ultrasonic signals in nondestructive testing," in *Proceedings of the SHM NDT Conference*, Saarbrücken, Germany, 2018.

[28] R. Lerch, G. Sessler, and D. Wolf, *Technische Akustik, Grundlagen und Anwendungen*, Springer, Berlin, Germany, 2009.